X-ray Crystal Structure of the Fe-Only Hydrogenase (CpI) from *Clostridium pasteurianum* to 1.8 Angstrom Resolution

John W. Peters,* William N. Lanzilotta, Brian J. Lemon, Lance C. Seefeldt

A three-dimensional structure for the monomeric iron-containing hydrogenase (CpI) from *Clostridium pasteurianum* was determined to 1.8 angstrom resolution by x-ray crystallography using multiwavelength anomalous dispersion (MAD) phasing. CpI, an enzyme that catalyzes the two-electron reduction of two protons to yield dihydrogen, was found to contain 20 gram atoms of iron per mole of protein, arranged into five distinct [Fe-S] clusters. The probable active-site cluster, previously termed the H-cluster, was found to be an unexpected arrangement of six iron atoms existing as a [4Fe-4S] cubane subcluster covalently bridged by a cysteinate thiol to a [2Fe] subcluster. The iron atoms of the [2Fe] subcluster both exist with an octahedral coordination geometry and are bridged to each other by three non-protein atoms, assigned as two sulfide atoms and one carbonyl or cyanide molecule. This structure provides insights into the mechanism of biological hydrogen activation and has broader implications for [Fe-S] cluster structure and function in biological systems.

The activation of molecular hydrogen constitutes a central reaction in the global biological energy cycle. This reaction is found among a diverse group of microorganisms where both the reduction of protons to yield hydrogen and the oxidation of hydrogen to yield protons have been widely characterized. Enzymes of the general class called hydrogenases are the catalysts responsible for most biological hydrogen activation. Hydrogenases are a diverse group of enzymes, often classified according to the transition metal cofactors associated with the protein. These metal center cofactors function both in the hydrogen activation reaction and in the transfer of electrons. Four groups of hydrogenases have thus far been identified according to their metal constitution: the NiFe, the NiFeSe, the Fe-only, and one enzyme that does not contain any bound transition metals (*1–3*). Of the hydrogenases that have been characterized to date, those containing Ni are most often involved in the oxidation of hydrogen. These enzymes have been observed in a broad range of microbes, including the methanogenic, photosynthetic, enteric, sulfate-reducing, and nitrogen-fixing bacteria [reviewed in (*1*)].

Recently, the x-ray crystal structure of a heterodimeric NiFe-containing hydrogenase isolated from the periplasm of the sulfate-reducing bacterium *Desulfovibrio gigas* was presented (*4*). The structure of the metal cluster responsible for hydrogen activation was found to be a bimetallic NiFe center covalently coordinated to the protein through four cysteinyl ligands. A mechanism for hydrogen binding and cleavage was proposed to involve an intermediate state in which hydrogen is bridged between both Fe and Ni at the active site (*5–6*).

The Fe-only hydrogenases have been identified in a small group of microbes, where they often catalyze the reduction of protons as a terminal electron acceptor to yield hydrogen. One such enzyme, the soluble, monomeric hydrogenase isolated from the Gram-positive anaerobe *Clostridium pasteurianum*, has been purified and extensively characterized both biochemically and spectroscopically [reviewed in (*2*)]. The most recent reports of quantitative Fe and S analysis indicate that this hydrogenase contains 20.1 ± 0.7 gram atoms of Fe per mole of protein and 17.8 ± 1.2 gram atoms of S^{2-} per mole of protein (*7*). Results from various spectroscopic methods have suggested that the Fe and S are organized into five distinct metal clusters. One of these, termed the H-cluster (hydrogen cluster), is proposed to be the site of hydrogen activation. Spectroscopic studies have indicated that this cluster is unlike any other [Fe-S] cluster that has been characterized to date (*2, 8*). Here, we used x-ray crystallographic methods to determine the structure of the *C. pasteurianum* Fe-only hydrogenase (CpI) to 1.8 Å resolution, revealing the structure of the active-site cluster.

Structure determination. The structure of CpI was solved by MAD phasing (*9*). Crystallization of CpI was accomplished using the microcapillary batch diffusion method (*10*). CpI crystallized in the tetragonal space group $P4_22_12$ with cell parameters $a = b =$ 111.6 Å, $c =$ 103.8 Å with one monomer in the asymmetric unit having a Matthews' coefficient of 2.6 or solvent content of 53% (*11*). For MAD phasing, data were collected at four different wavelengths such that dispersive and Bijvoet differences were maximized from 20 native Fe atoms (*12*) (Table 1). As expected, the anomalous differences were significant because of the presence of 20 Fe atoms per ~60 kD of protein (Table 2). The cluster sites were initially identified by the Patterson method, and upon solvent flattening, the phases were improved such that the protein envelope was clearly visible in electron density maps. MAD phasing to the full resolution of the data (2.5 Å) was obtained by iterative assignment of individual Fe atoms on the basis of the limited degrees of freedom in the clusters of known composition and the location of the clusters in the initial electron density maps. High-quality electron density maps were obtained from the individual refinement of 16 of the 20 possible Fe atoms, and upon subsequent solvent flattening, all 574 residues could be assigned (*13*). The additional metal cluster atoms were assigned in subsequent $2F_{obs} - F_{calc}$ electron density maps and refined omit $F_{obs} - F_{calc}$ electron density maps. Through several cycles of manual model building and refinement, a final model was produced. The model has been refined to 1.8 Å resolution to a current R_{cryst} of 0.180 and R_{free} of 0.235 (Tables 1 and 2).

Overall structure. The overall structure of CpI resembles a mushroom (Fig. 1A), with a large cap connected to a stem. This overall structure can be subdivided into four distinct nonoverlapping domains. The largest of the four domains, designated the active-site domain, makes up the mushroom cap; the remaining three smaller domains constitute the stem, which contains the accessory [Fe-S] clusters termed FS4A, FS4B, FS4C, and FS2 (Fig. 1B). The active-site domain contains about two-thirds of the total protein (amino acid residues 210 to 574). The fold of the active-site domain consists of two four-stranded twisted β sheets, each flanked by a number of α helices that appear to be two nearly equivalent lobes, with one β sheet and associated helices contained within each lobe. The active-site cluster (abbreviated HC) is located at the interface of the two lobes near the site of interaction with the remaining domains. The left lobe of the active-site domain (Fig. 1A) contains a four-stranded parallel β sheet formed from β strands including

The authors are in the Department of Chemistry and Biochemistry, Utah State University, Logan, UT 84322, USA.

*To whom correspondence should be addressed. E-mail: petersj@cc.usu.edu

residues 223 to 230, 263 to 268, 346 to 354, and 376 to 380. Similarly, the right lobe of the active-site domain (Fig. 1A) contains a four-stranded mixed β sheet that includes β strands defined by residues 294 to 297, 453 to 461, 465 to 473, and 490 to 498. The active-site cluster is located in a cleft that makes a clear division spanning the entire domain.

The active-site cluster provides a site of covalent attachment between the two lobes of the active-site domain. The attachment of the cluster occurs at the interface of the two β sheets at loop regions adjacent to three β strands, two from the left lobe and one from the right lobe (Fig. 2A). These regions exhibit a high degree of conservation in sequence alignments of known Fe-only hydrogenases and putative Fe-only hydrogenases (*14, 15*).

The remaining domains each contain [Fe-S] clusters. The domain directly interacting with the active-site domain contains two clusters of the [4Fe-4S] type, designated FS4A and FS4B. FS4A is the cluster closest to the active-site H-cluster (~9 Å edge-to-edge) and thus probably represents the direct electron donor to the active-site H-cluster. The FS4B cluster is ~10 Å away from the FS4A cluster, suggesting an in-line electron transfer pathway from FS4B to FS4A to HC. The remaining two domains contact the FS4A-FS4B domain. One of these contains a single cluster of the [2Fe-2S] type (designated the FS2 domain). The other contains a single [4Fe-4S] cluster with an unusual mixed cysteine and histidine ligation (designated the FS4C domain). The relative positions of each metal cluster are shown in Fig. 1B. The possible roles of each of the metal clusters in the hydrogenase mechanism are discussed below.

Active-site cluster. The H-cluster (Fig. 2B) contains six Fe atoms arranged as a [4Fe-4S] subcluster bridged to a [2Fe] subcluster by a single cysteinyl S. This arrangement is markedly different from previously observed biological metal clusters, model compounds, and proposed clusters (*16*). The [4Fe-4S] subcluster is coordinated to the protein through four cysteines, one of which acts as the bridge to the other subcluster. The [2Fe] subcluster consists of two octahedrally liganded Fe atoms that together contain five CO/CN ligands (modeled as CO here), three S ligands (one of which is cysteine S), and one H_2O ligand. The ability of multiple carbonyls to adopt an octahedral geometry about two bridged Fe atoms is well established in the structure of a nonacarbonyl di-Fe complex and related compounds (*17*). More recently, a relevant di-Fe complex containing bridged, octahedrally coordinated Fe with mixed ligation has been presented (*18*); however, the composition of the ligands is different from that observed here.

The assignment of CO or CN as ligands to the Fe atoms of the H-cluster is based in part on the presence of such ligands to the Fe atom of the NiFe hydrogenase active site (*19*). Fourier transform infrared spectroscopy studies indicate that several Fe-only hydrogenases are likely to have CN or CO as terminal ligands to a metal cluster, as was observed for the NiFe hydrogenase (*20*). In the present study, CO and CN, being of nearly equivalent atomic mass, could not be distinguished from each other given their similar expected electron density. S and CO/CN could be distinguished by differential refinement at each metal site individually, resulting in clear dif-

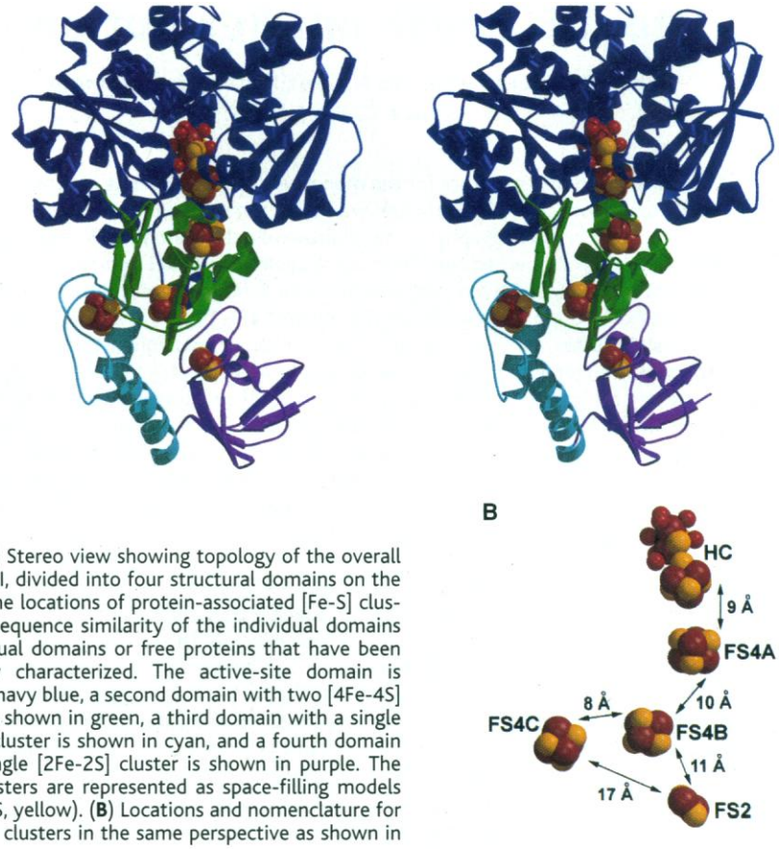

Fig. 1. (**A**) Stereo view showing topology of the overall fold of CpI, divided into four structural domains on the basis of the locations of protein-associated [Fe-S] clusters and sequence similarity of the individual domains to individual domains or free proteins that have been previously characterized. The active-site domain is shown in navy blue, a second domain with two [4Fe-4S] clusters is shown in green, a third domain with a single [4Fe-4S] cluster is shown in cyan, and a fourth domain with a single [2Fe-2S] cluster is shown in purple. The [Fe-S] clusters are represented as space-filling models (Fe, rust; S, yellow). (**B**) Locations and nomenclature for the [Fe-S] clusters in the same perspective as shown in (A).

Table 1. Data and refinement statistics.

Data statistics				
Wavelength (Å)	Resolution range (Å)	Unique reflections	Completeness (%)	R_{merge}
1.9074	20.0–2.5	21,323	92.1	0.039
1.7418	20.0–2.5	22,050	95.3	0.046
1.7398	20.0–2.5	21,830	94.3	0.066
1.5498	20.0–2.5	22,529	97.3	0.054
1.5418	20.0–1.8	54,582	90.1	0.067

Refinement statistics	
Protein non-hydrogen atoms	5537
Solvent molecules	776
Resolution range (Å)	20.0 to 1.8
Total reflections ($F > 1\sigma F$)	52,333
Total reflections used in R_{free}	2647
R_{cryst}	0.180
R_{free}	0.235
Rmsd of bond distances (Å)	0.009
Rmsd of angles (°)	2.21
Average *B*–protein and metal clusters (Å^2)	12.4
Average *B*–solvent (Å^2)	36.9

$R_{merge} = \Sigma_{hkl}[\Sigma_i(|I_{hkl,i} - \langle I_{hkl}\rangle|)]/\Sigma_{hkl,i}\langle I_{hkl}\rangle$, where I_{hkl} is the intensity of an individual measurement of the reflection with indices hkl and $\langle I_{hkl}\rangle$ is the mean intensity of that reflection.

ferences in the fit of the model to the experimental data evident in $F_{obs} - F_{calc}$ electron density maps and B factors. In the model, the Fe proximal to the [4Fe-4S] subcluster (HC [2Fe] subcluster Fe1) is covalently coordinated to the protein only through the bridging S of Cys^{503}. In contrast, the distal Fe (HC [2Fe] subcluster Fe2) has no direct covalent attachment to the protein (Fig. 2C). Within the [2Fe] subcluster, each Fe atom is bridged to the other by two S atoms and one CO or CN molecule. These three bridging ligands deviate somewhat from the true octahedral geometry. The S atoms refine to a slightly shorter distance to one another than to the bridging CO or CN molecule, probably (at least in part) as a result of the heterogeneity of these ligands. Additionally, both experimentally phased electron density maps and subsequent $2F_{obs} - F_{calc}$ electron density maps indicate the two bridging S atoms themselves are bridged by an atom or atoms of unknown identity. This has been refined as a single water molecule. However, upon refinement, the appearance of positive difference density in $F_{obs} - F_{calc}$ electron density maps at this position suggests that this region represents an atom of larger electron density, more than one covalently bound light atom, or multiple sites that are fractionally occupied by water. The four terminally ligated CO/CN molecules (two on each Fe of the [2Fe] subcluster) are all located on the same side of the cluster as the bridging CO/CN. In the structure of the NiFe hydrogenase, the active site consists of a five-coordinate Ni atom and an Fe atom that has a similar octahedral arrangement, as is shown here. The S ligands of the Fe of the NiFe hydrogenase are supplied by cysteine residues that provide the sites of direct covalent attachment of the active-site cluster to the protein.

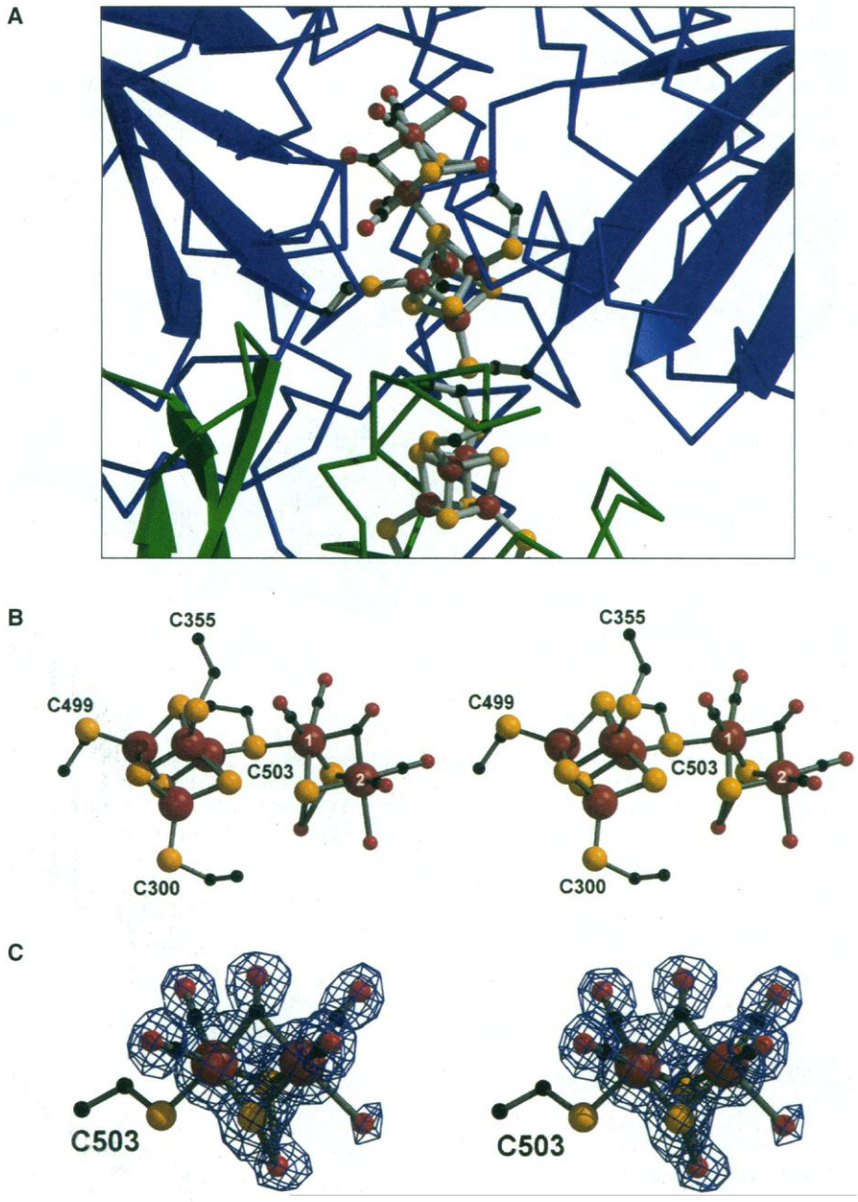

Fig. 2. (**A**) The active-site cluster or H-cluster (HC) within its polypeptide environment, showing the location of the β sheets of each lobe of the active-site domain. The β strands of the two β sheets are represented in topology diagram form, and the remaining topology of the protein is represented as an α-carbon trace. Ligation to the active-site cluster (ball-and-stick) is provided by Cys residues that are located in loop regions adjacent to the β strands of the β sheets and provide a site of covalent attachment of the two lobes in this region. The view is in the same orientation as that of Fig. 1A, and it can be seen that the [4Fe-4S] subcluster of HC is located in close proximity to the FS4A [4Fe-4S] cluster of the FS4A-FS4B domain for electron transfer. (**B**) Stereo view of the CpI HC and coordinating Cys ligands located at the boundary of the two lobes of the active-site domain. The active-site cluster is covalently bound to the proteins through four cysteine S atoms (yellow) that are bound to five Fe atoms (rust). The CO/CN molecules, which serve as ligands to the [2Fe] subcluster of the active-site cluster, are all represented as carbonyls (C, black; O, red). The two Fe atoms are labeled 1 and 2 (see text) and are located at a refined distance of 2.62 Å with respect to one another. Additional ligands to the Fe atoms of this subcluster include two bridging S atoms (yellow) and a terminally bound water molecule (red). A water molecule (red) is also shown linking the bridging S atoms. (**C**) Stereo view of 1.8 Å resolution $F_{obs} - F_{calc}$ omit map (navy blue), contoured at 5σ, of the [2Fe] subcluster of the active-site cluster.

The [4Fe-4S] subcluster of the active site is ligated to the protein through Cys^{300}, Cys^{355}, and Cys^{499} as well as the subcluster-bridging Cys^{503}. The linkage of a [4Fe-4S] cluster to another metal-containing prosthetic group is reminiscent of the active site of sulfite reductase, where a [4Fe-4S] cluster is bridged in the same manner to the Fe of a seroheme (*21*). The proposed active-site cluster of carbon monoxide dehydrogenase has been suggested to consist of a [4Fe-4S] cluster bridged to a single Ni atom by the S of a cysteine residue (*22*). The close association of the HC [2Fe] subcluster with its [4Fe-4S] subcluster is consistent with a recent interpretation of Mössbauer spectra suggesting that HC could consist of one or two Fe atoms exchange-coupled to a [4Fe-4S] cluster (*23*).

Accessory cluster domains. The remaining Fe atoms of CpI are organized into four clusters (three [4Fe-4S] clusters and one [2Fe-2S] cluster) that are arranged into three domains. The FS2 domain consists of two nearly perpendicular mixed β sheets and a single α helix containing a [2Fe-2S] cluster coordinated by Cys^{33}, Cys^{46}, Cys^{49}, and Cys^{62}. The presence of a [2Fe-2S] cluster in CpI independent of the active-site cluster was indicated from the results of resonance Raman studies (*24, 25*). Additionally, sequence comparison of the NH_2-terminal portion of

this domain reveals considerable sequence similarity to a number of [2Fe-2S] ferredoxins, including the arrangement of cysteine residues involved in coordination of the [2Fe-2S] cluster. As expected, the conservation in sequence translates to conservation in the overall fold of this domain, such that all the main elements of the domain (the perpendicular β sheets and α helix) are similar when compared to the [2Fe-2S] ferredoxin from *Chlorella fusca* (*26*) (Fig. 3A). The [2Fe-2S] cluster is close to the surface of the domain and is a possible site for interaction with electron donors.

The FS4A-FS4B domain is immediately adjacent to the active-site domain and contains two [4Fe-4S] clusters, each coordinated by four cysteine residues. The FS4A cluster is coordinated by Cys^{157}, Cys^{190}, Cys^{193}, and Cys^{196} and the FS4B cluster is coordinated by Cys^{147}, Cys^{150}, Cys^{153}, and Cys^{200} of the amino acid sequence. As for the FS2 domain, the sequence for this domain shows similarities to a number of ferredoxins containing two [4Fe-4S] clusters, including a distinctive arrangement of cysteine residues with two sets of Cys-X-X-Cys-X-X-Cys-X-X-X-Cys sequences (where each X indicates an amino acid other than Cys). The similarity is also evident in the conservation of the overall fold of the domain, as illustrated in a side-by-side comparison with the related ferredoxin from *Chromatium vinosum* (*26, 27*) (Fig. 3B). Each Cys-X-X-Cys-X-X-Cys-X-X-X-Cys motif provides three cysteinyl ligands to one of the [4Fe-4S] clusters and one cysteinyl ligand to the second cluster, such that the clusters are intimately linked by a short turn of an α helix.

The FS4A-FS4B domain is linked to the NH_2-terminal FS2 domain by the FS4C domain, a short domain consisting of two α helices linked by a loop region that binds a single [4Fe-4S] cluster. The [4Fe-4S] cluster has three cysteinyl ligands and a single histidine ligand provided by His^{94}, Cys^{98}, Cys^{101}, and Cys^{107} of the sequence (Fig. 3C). Histidine ligation of a [4Fe-4S] cluster has been observed in the structure of the NiFe hydrogenase from *D. gigas* (*1*). The coordination of Fe by histidine in CpI was anticipated; however, this was suggested to be associated with the active-site cluster (*28*). Histidine ligation has been observed in the [2Fe-2S]–containing Rieske proteins, which have higher midpoint potentials than that of the similar [2Fe-2S] clusters that are coordinated exclusively by cysteinyl ligands (*29*). This suggests that a role of the single histidine ligand in the [4Fe-4S] cluster of the FS4C domain may be to tune the midpoint potential to accommodate an appropriate electron donor. However, experimental evidence suggests that the midpoint potentials of all the accessory clusters of CpI are equivalent at −420 mV (*30*). Interestingly, the Nε of His^{94} is the site of binding to the Fe. This is in contrast with all previous examples of His ligands to an [Fe-S] cluster, where the Nδ atom of histidine is coordinating. FS4C, like FS2, is near the protein surface and thus may participate in intermolecular electron transfer with redox partners of CpI.

The relative location of each of the metal clusters within CpI reveals potential electron transfer pathways. As mentioned earlier, FS4B, FS4A, and HC appear to form a sequential electron transfer pathway with covalent or H-bonding connections between each cluster (Fig. 4). FS4B appears to sit as a junction point, accepting electrons from either FS4C or FS2. Because the latter two clusters are located near the protein surface, they are possible initial electron acceptors from the physiological electron donors.

Active-site environment. In addition to the four covalent cysteinyl ligands, there are a number of additional residues that define the active-site environment. Although only the single bridging ligand is involved in di-

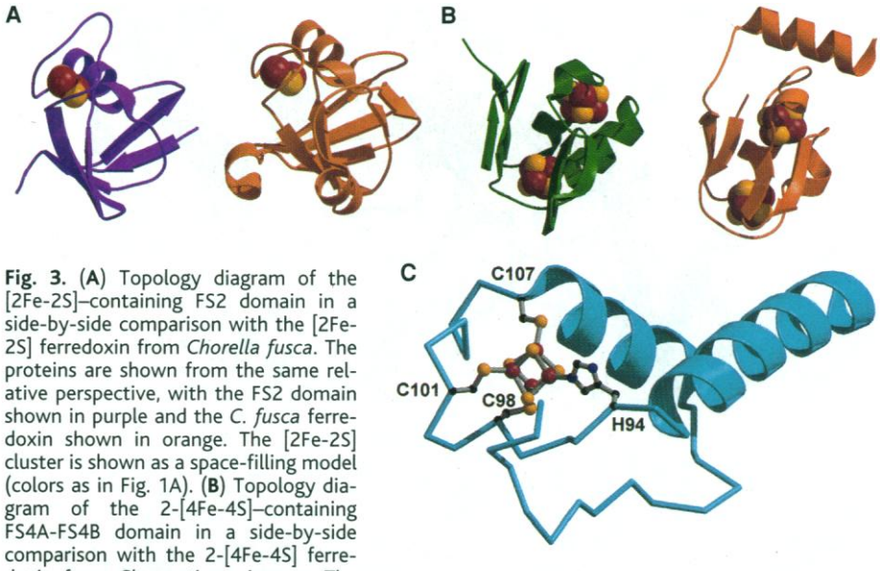

Fig. 3. (**A**) Topology diagram of the [2Fe-2S]–containing FS2 domain in a side-by-side comparison with the [2Fe-2S] ferredoxin from *Chorella fusca*. The proteins are shown from the same relative perspective, with the FS2 domain shown in purple and the *C. fusca* ferredoxin shown in orange. The [2Fe-2S] cluster is shown as a space-filling model (colors as in Fig. 1A). (**B**) Topology diagram of the 2-[4Fe-4S]–containing FS4A-FS4B domain in a side-by-side comparison with the 2-[4Fe-4S] ferredoxin from *Chromatium vinosum*. The proteins are shown from the same relative perspective, with the FS4A-FS4B domain shown in green and the *C. vinosum* ferredoxin shown in orange. The [4Fe-4S] clusters are shown as space-filling models. (**C**) Topology diagram of the [4Fe-4S]–containing FS4C domain, showing the location and composition of the four coordinating ligands His^{94}, Cys^{98}, Cys^{101}, and Cys^{107}.

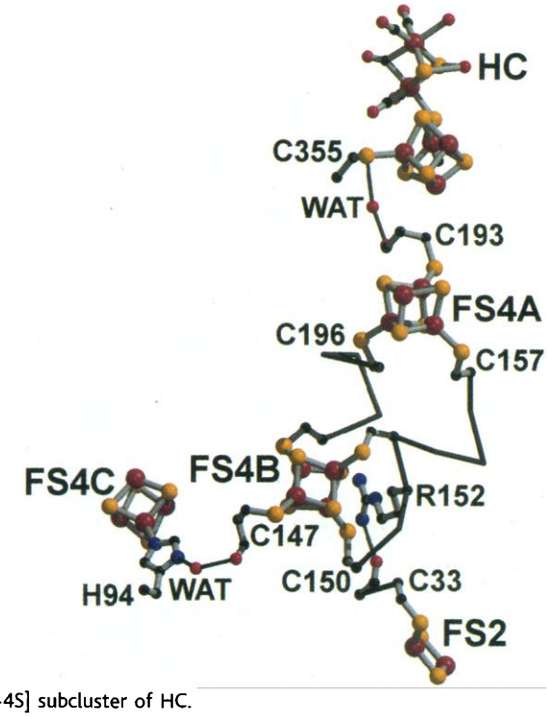

Fig. 4. Potential electron transfer pathways from the [2Fe-2S] cluster of the FS2 domain and the [4Fe-4S] cluster of the FS4C domain to the active-site cluster via the two [4Fe-4S] clusters of the FS4A-FS4B domain. The [2Fe-2S] cluster of the FS2 domain is linked to the [4Fe-4S] cluster FS4A through a hydrogen bond from the peptide-bond carbonyl of the [2Fe-2S] cluster ligand Cys^{33} to Arg^{152} located between the Cys^{150} and Cys^{153} ligands of FS4B. The [4Fe-4S] cluster of the FS4C domain is linked through hydrogen bonding of the δN of the His^{94} ligand to the peptide-bond carbonyl of Leu^{146} adjacent to the Cys^{147} ligand of FS4B mediated by a water molecule. The FS4B cluster is intimately linked to FS4A in two equivalent locations by turns of two α helices. The coordinating ligand Cys^{153} of FS4B is linked to the Cys^{157} of FS4A, and in an analogous fashion Cys^{200} of FS4B is linked to Cys^{196} of FS4A. The FS4A cluster is then in turn linked to the HC by hydrogen bonding of the peptide-bond carbonyl of the Cys^{193} ligand to FS4A to the Cys^{355} S of the [4Fe-4S] subcluster of HC.

rectly coordinating the [2Fe] subcluster, the binding pocket is structurally well defined, suggesting that the cluster is fixed in space. Two methionine residues (Met^{353} and Met^{497}) are located near the H-cluster (Fig. 5). Both of these Met residues are conserved within the sequence when compared to the other known Fe-only hydrogenases (*14*). The sulfur atom of Met^{497} is ~3.4 Å away from the atom(s) connecting the two bridging sulfur atoms of the [2Fe] subcluster. The sulfur atom of Met^{353} is located ~3.2 Å from the CO/CN that bridges Fe1 and Fe2. Other amino acid side chains in close proximity to the terminal CO/CN ligands include Nζ of Lys^{358} and Oγ of Ser^{232}, both ~2.9 Å away from these ligands. The adjacent Pro^{231} is one of a number of hydrophobic residues that surround Fe2, potentially protecting the cluster from solvent access and regulating the availability of substrates such as protons. Additional hydrophobic residues in the polypeptide environment of Fe2 include Ile^{268}, Ala^{272}, Pro^{324}, Phe^{417}, and Val^{423}. The peptide-bond carbonyl of Phe^{417} is ~3.4 Å from one of the bridging sulfurs of the [2Fe] subcluster. The other bridging sulfur atom in the subcluster is in close proximity to the peptide-bond carbonyl of Cys^{299}. A free cysteinyl residue (Cys^{299}) is ~5 Å from Fe2 of the [2Fe] subcluster and ~3 Å from the terminally bound water molecule.

Proton reduction by CpI. The location of the free cysteine residue, Cys^{299}, with respect to the cluster-bound water is suggestive of a potential mechanism of proton reduction catalyzed by CpI. An important function for this amino acid is supported by the strict conservation of a comparable Cys in the sequences of all known Fe-only hydrogenases (*14*). Although the purification and crystallization of CpI was accomplished in the presence of reductant, it was likely to be consumed over the course of the period of crystal growth. If this were indeed the case, the enzyme could be in an oxidized state. With the exception of the terminally bound water molecule, the remaining ligands (CO/CN and S) should be very strong ligands. If we are indeed examining the oxidized state of CpI, a reasonable mechanism for proton reduction at this active site might be the displacement of the terminal water ligand bound to Fe2 upon reduction, with the subsequent generation of an Fe-hydride intermediate. Cys^{299} could act as a proton donor for the formation of dihydrogen. The pK_a [–log K_a (acid dissociation constant)] of free Cys (~8.0) would allow this residue to act as a general acid/base near physiological pH values. Such a mechanism would be consistent with the heterolytic cleavage of hydrogen inferred from isotope studies (*31*). CpI has been shown to undergo irreversible inactivation in the presence of CO (*2, 7, 30, 32*). It is easy to envision that the binding of CO displaces the terminally bound water molecule of Fe2, and this would result in the inhibition of proton reduction by our proposed mechanism.

A potential pathway of proton transfer exists from Cys^{299} 12 Å to the protein surface, involving two Glu residues, a Ser residue, and a water molecule. There are no free cysteines in close proximity to the active site of the *D. gigas* NiFe hydrogenase; in contrast, there are a number of His residues in the active-site environment, presumably acting as proton acceptors (*4*). This difference in the two active-site environments may support the preference in the direction in which they catalyze reversible hydrogen oxidation physiologically. Additionally, Ni at the active site may also contribute to the preference for hydrogen oxidation over hydrogen evolution in the Ni-containing hydrogenases (*1*). *Clostridium pasteurianum* has been shown to express another Fe-only hydrogenase, CpII; however, this enzyme functions as an uptake hydrogenase preferentially catalyzing hydrogen oxidation. Differences in the observed midpoint potentials of the active-site clusters of CpI and CpII with respect to their associated accessory clusters may account for the different directions of electron flow to or from the H-cluster in the presence of the appropriate oxidized or reduced electron carriers (*16*). Differences in spectroscopic properties and CO inhibition of CpI and CpII suggest that the mechanisms of hydrogen activation catalyzed by CpI and CpII are distinct (*30*). The

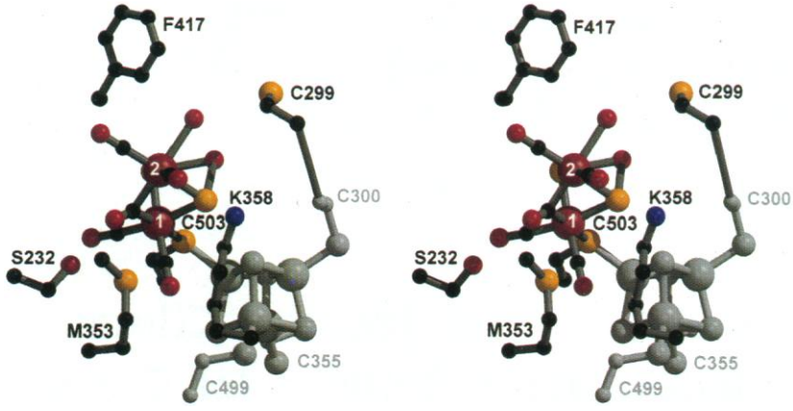

Fig. 5. Stereo view of selected amino acid residues in the polypeptide environment of the [2Fe] subcluster of HC (colors as in Fig. 2). The [4Fe-4S] subcluster and associated ligand are included to provide the proper perspective and are indicated in light gray. C, Cys; F, Phe; K, Lys; S, Ser; M, Met.

Table 2. Anomalous diffraction differences and scattering factors for the CpI crystal used for MAD phasing (*9*). Observed diffraction ratios represent $\langle\Delta|F|^2\rangle^{1/2}/\langle|F|^2\rangle^{1/2}$, where $\Delta|F|$ is the absolute value of the Bijvoet differences at one wavelength (along the diagonal) or the dispersive difference between intersecting wavelengths (off-diagonal elements). An estimate of the noise in the anomalous signals is indicated by the Bijvoet differences for centric reflections shown in parentheses for each wavelength. The scattering factors were refined after multiple MADLSQ cycles (*33*); the f' and f'' values for the pre-edge wavelength (1.9074 Å) were fixed at the theoretical values, −2.18 and 0.55, respectively.

Wavelength (Å)	Observed ratio (30.0 > d > 6.0 Å)				Observed ratio (6.0 > d > 3.5 Å)				Observed ratio (3.5 > d > 2.5 Å)				Scattering factors (e)	
	1.9074	1.7418	1.7398	1.5498	1.9074	1.7418	1.7398	1.5498	1.9074	1.7418	1.7398	1.5498	f'	f''
1.9074	0.038 (0.020)	0.089	0.073	0.038	0.035 (0.028)	0.058	0.054	0.034	0.048 (0.038)	0.069	0.066	0.053	−2.18	0.55
1.7418		0.071 (0.025)	0.032	0.105		0.043 (0.027)	0.023	0.058		0.056 (0.044)	0.041	0.079	−8.13	2.59
1.7398			0.107 (0.027)	0.089			0.059 (0.030)	0.053			0.076 (0.047)	0.075	−7.43	3.80
1.5498				0.085 (0.028)				0.054 (0.029)				0.067 (0.043)	−1.28	3.11

structural characterization of CO-inhibited forms of CpI, as well as that of CpII and other Fe-only and NiFe hydrogenases, may contribute additional insights to the mechanistic details of reversible hydrogen oxidation catalyzed by the hydrogenase enzymes.

References and Notes

1. A. E. Pryzbyla, J. Robbins, N. Menon, H. D. Peck, *FEMS Microbiol. Rev.* **88**, 109 (1992).
2. M. W. W. Adams, *Biochim. Biophys. Acta* **1020**, 115 (1990).
3. R. K. Thauer, A. R. Klein, G. C. Hartmann, *Chem. Rev.* **96**, 3031 (1996).
4. A. Volbeda *et al.*, *Nature* **373**, 580 (1995).
5. J. C. Fontecilla-Camps, *J. Biol. Inorg. Chem.* **1**, 91 (1996).
6. A. Volbeda *et al.*, *J. Am. Chem. Soc.* **118**, 12989 (1996).
7. M. W. W. Adams, E. Eccleston, J. B. Howard, *Proc. Natl. Acad. Sci. U.S.A.* **86**, 4932 (1989).
8. A. T. Kowal, M. W. W. Adams, M. K. Johnson, *J. Biol. Chem.* **264**, 4342 (1989).
9. W. A. Hendrickson, *Science* **254**, 51 (1991).
10. CpI was purified from *C. pasteurianum* as described [J.-S. Chen and L. E. Mortenson, *Biochim. Biophys. Acta* **371**, 283 (1974)] with hydrogen evolution activity of 3400 μmol min^{-1} mg^{-1}. Crystallization was accomplished using the microcapillary batch diffusion method [M. M. Georgiadis, *Science* **257**, 1653 (1992)] and a precipitating solution of 25% polyethylene glycol 4000, 0.1 M sodium acetate (pH 4.6), and 0.2 M ammonium sulfate. The precipitating solution was allowed to slowly equilibrate with the protein solution [50 mM tris (pH 8.0) and 0.2 M KCl], resulting in a crystallization solution at an approximate pH of 5.1, which is near the pH optimum for hydrogen evolution activity of CpI at pH 5.0 [V. M. Fernández, *Anal. Biochem.* **130**, 54 (1983)]. Because of the oxygen sensitivity of CpI, sodium dithionite was used as a reductant to remove trace amounts of oxygen in both the precipitating solution and the protein samples. All manipulations were conducted in a vacuum atmospheres anaerobic chamber under an atmosphere of 100% N_2 at room temperature.
11. B. W. Matthews, *J. Mol. Biol.* **33**, 491 (1968).
12. For data collection, the crystals were equilibrated in a mother liquor solution (containing a final concentration of ~10% glycerol) and cooled to near liquid N_2 temperatures. Data for MAD phasing were collected at Stanford Synchrotron Radiation Laboratory (SSRL) beam line 1-5 equipped with a Hamlin charge-coupled device detector. The individual images were indexed using REFIX [W. Kabsch, *J. Appl. Crystallogr.* **24**, 795 (1993)], and the data were processed with MOSFLM [A. G. W. Leslie, *CCP4 and ESF-EACMB Newsletter on Protein Crystallography* (1992), p. 26] and scaled with SCALA of the CCP4 suite of crystallography software [Collaborative Computational Project No. 4, *Acta Crystallogr.* **D50**, 760 (1994)]. The 1.8 Å resolution data used in the final refinement were collected with Cu-K α radiation using a Rigaku RU300 x-ray generator equipped with a RAXIS-IIc phosphorimaging plate detector. The data were processed with DENZO and scaled with SCALEPACK [Z. Otwinowski, in *Data Collection and Processing*, L. Sawyer, N. Isaacs, S. Bailey, Eds. (CCP4 Study Weekend, SERC Daresbury Laboratory, Warrington, UK, 1991), pp. 56–62].
13. Initial Fe-S cluster sites could be identified using the program SOLVE [T. C. Terwilliger, *Acta Crystallogr.* **D50**, 17 (1994)], but even upon solvent flattening by SOLOMON [J. P. Abrahams and A. G. W. Leslie, *ibid.* **D52**, 30 (1996)] they were not interpretable with respect to the positions of individual amino acids; however, upon solvent flattening, the protein envelope was clearly visible. High-resolution phasing was obtained by assignment of the positions of the individual Fe atoms based on the limited degrees of freedom with respect to several of the clusters of known composition and the apparent sites of interaction between the protein and these clusters in the initial electron density maps (J. W. Peters and H. Bellamy, in preparation). When 16 Fe atoms were assigned with a reasonably high degree of certainty and were refined against the anomalous data, phasing could be extended to the full resolution of the MAD data (2.5 Å) and high-quality electron density maps were obtained upon solvent flattening. The high-quality initial electron density maps (calculated to 3.0 Å resolution) allowed all amino acid residues (574) of the sequence (*15*) and metal atoms to be placed with a high degree of certainty using the program O [T. A. Jones, J. Y. Zhou, S. W. Cowan, M. Kjeldgaard, *Acta Crystallogr.* **A47**, 110 (1991)]. Several rounds of positional and *B*-factor refinement [A. T. Brünger, J. Kuriyan, M. Karplus, *Science* **235**, 258 (1987)] of this initial model against the 1.8 Å resolution native data resulted in an R_{cryst} of 0.274 and an R_{free} of 0.313. This model was improved by iterative manual model building against $2F_{obs} - F_{calc}$ electron density maps and subsequent refinement. The present model exhibits good geometry, with 100% of the amino acid residues located in either most favorable or additionally allowed regions of the Ramachandran plot, as calculated with PROCHECK [R. A. Laskowski, M. W. McArthur, M. W. Moss, J. M. Thornton, *J. Appl. Crystallogr.* **26**, 283 (1993)]. The program PROMOTIF was used for secondary structure assignments [E. G. Hutchinson and J. M. Thornton, *Protein Sci.* **5**, 212 (1996)].
14. M. F. Gorwa, C. Croux, P. Soucaille, *J. Bacteriol.* **178**, 2668 (1996); S. Malki *et al.*, *ibid.* **177**, 2628 (1995); J. D. Santangelo, P. Durre, D. R. Woods, *Microbiology* **141**, 171 (1995); J. Stokkermans, W. van Dohngen, A. Kaan, W. van den Berg, C. Veeger, *FEMS Microbiol. Lett.* **58**, 217 (1989); G. Voordouw and S. Brenner, *Eur. J. Biochem.* **148**, 515 (1985); G. Voordouw, J. D. Strang, F. R. Wilson, *J. Bacteriol.* **171**, 3881 (1989).
15. J. Meyer and J. Gagnon, *Biochemistry* **30**, 9697 (1991).
16. R. H. Holm, P. Kennepohl, E. I. Solomon, *Chem. Rev.* **96**, 2239 (1996).
17. F. A. Cotton and G. Wilkinson, *Advanced Inorganic Chemistry* (Wiley, New York, 1988).
18. V. E. Kaasjager *et al.*, *Angew. Chem. Int. Ed.* **37**, 1668 (1998).
19. R. P. Happe, W. Roseboom, A. J. Pierik, S. P. J. Albracht, *Nature* **385**, 126 (1997).
20. T. M. Van Der Spek, *Eur. J. Biochem.* **237**, 629 (1996).
21. B. R. Crane, L. M. Siegel, E. D. Getzoff, *Science* **270**, 59 (1995).
22. H. Beinhart, R. H. Holm, E. Münck, *ibid.* **277**, 653 (1997).
23. J. Xia, Z. Hu, C. V. Popescu, P. A. Lindahl, E. Münck, *J. Am. Chem. Soc.* **119**, 8301 (1997).
24. K. A. Macor, R. S. Czernuszewicz, M. W. W. Adams, T. G. Spiro, *J. Biol. Chem.* **262**, 9945 (1987).
25. W. Fu *et al.*, *Biochemistry* **32**, 4813 (1993).
26. Brookhaven Protein Data Bank accession codes for the [2Fe-2S] ferredoxin from *Chlorella fusca* and the 2-[4Fe-4S] ferredoxin from *Chromatium vinosum* are 1awd and 1blu, respectively.
27. J. M. Moulis, L. C. Seiker, K. S. Wilson, Z. Dauter, *Protein Sci.* **5**, 1765 (1996).
28. H. Thomann, M. Bernardo, M. W. W. Adams, *J. Am. Chem. Soc.* **113**, 7044 (1991).
29. P. J. Stephens, D. R. Jollie, A. Warshel, *Chem. Rev.* **96**, 2491 (1996).
30. M. W. W. Adams, *J. Biol. Chem.* **262**, 15054 (1987).
31. ———, L. E. Mortenson, J.-S. Chen, *Biochim. Biophys. Acta* **594**, 105 (1980).
32. R. K. Thauer, B. Käufer, M. Zähringer, K. Jungermann, *Eur. J. Biochem.* **42**, 447 (1974).
33. W. I. Weis, R. Kahn, K. Drickamer, W. A. Hendrickson, *Science* **254**, 1608 (1991).

34. We thank H. Bellamy of SSRL for assistance in MAD data collection; F. Whitby and C. Hill of the University of Utah for use of their data collection facility for collection of preliminary data; and L. Berreau, S. Ensign, R. Holz, and J. Hubbard for helpful discussions. All figures were produced using MOLSCRIPT [P. J. Kraulis, *J. Appl. Crystallogr.* **24**, 946 (1991)] and RASTER3D [D. Bacon and W. F. Anderson, *J. Mol. Graphics* **6**, 219 (1988); E. A. Merritt and M. E. P. Murphy, *Acta Crystallogr.* **D50**, 869 (1994)]. Supported by NSF grants MCB-9807821 (J.W.P.) and MCB-9722937 (L.C.S.) and American Chemical Society–Petroleum Research Fund grant 33183-G4 (J.W.P.). The data collection facility at SSRL is funded by the U.S. Department of Energy, Office of Basic Energy Sciences, and by the NIH Biomedical Research Technology Program, Division of Research Resources. Coordinates have been deposited in the Brookhaven Protein Data Bank (accession code 1feh).

25 September 1998; accepted 30 October 1998

A 25,000-Year Tropical Climate History from Bolivian Ice Cores

L. G. Thompson, M. E. Davis, E. Mosley-Thompson, T. A. Sowers, K. A. Henderson, V. S. Zagorodnov, P.-N. Lin, V. N. Mikhalenko, R. K. Campen, J. F. Bolzan, J. Cole-Dai, B. Francou

Ice cores that were recovered from the summit of Sajama mountain in Bolivia provide carbon-14–dated tropical records and extend to the Late Glacial Stage (LGS). Oxygen isotopic ratios of the ice decreased 5.4 per mil between the early Holocene and the Last Glacial Maximum, which is consistent with values from other ice cores. The abrupt onset and termination of a Younger Dryas–type event suggest atmospheric processes as the probable drivers. Regional accumulation increased during the LGS, during deglaciation, and over the past 3000 years, which is concurrent with higher water levels in regional paleolakes. Unlike polar cores, Sajama glacial ice contains eight times less dust than the Holocene ice, which reflects wetter conditions and extensive snow cover.

A knowledge of tropical sensitivity to global paleoclimate changes and the abruptness of past changes is essential for modeling how the Earth's climate system responds during glacial stages and for simulating future climatic scenarios under warmer conditions that are anticipated from enhanced greenhouse gas concentrations (*1*). Recent research suggests that tropical proxy records may be more representative of global mean annual temperatures than proxy records from higher latitudes (*2*).